INTERNATIONAL JOURNAL FOR NUMERICAL METHODS IN FLUIDS
Int. J. Numer. Meth. Fluids **28**: 129–142 (1998)

A SPECTRAL–FINITE DIFFERENCE SOLUTION OF THE NAVIER–STOKES EQUATIONS IN THREE DIMENSIONS

GIANCARLO ALFONSI*, GIUSEPPE PASSONI, LEA PANCALDO AND DOMENICO ZAMPAGLIONE

Dipartimento di Ingegneria Idraulica, Ambientale e del Rilevamento, Politecnico di Milano, Piazza Leonardo da Vinci 32, 20133 Milano, Italy

SUMMARY

A new computational code for the numerical integration of the three-dimensional Navier–Stokes equations in their non-dimensional velocity–pressure formulation is presented. The system of non-linear partial differential equations governing the time-dependent flow of a viscous incompressible fluid in a channel is managed by means of a mixed spectral–finite difference method, in which different numerical techniques are applied: Fourier decomposition is used along the homogeneous directions, second-order Crank–Nicolson algorithms are employed for the spatial derivatives in the direction orthogonal to the solid walls and a fourth-order Runge–Kutta procedure is implemented for both the calculation of the convective term and the time advancement. The pressure problem, cast in the Helmholtz form, is solved with the use of a cyclic reduction procedure. No-slip boundary conditions are used at the walls of the channel and cyclic conditions are imposed at the other boundaries of the computing domain.

Results are provided for different values of the Reynolds number at several time steps of integration and are compared with results obtained by other authors. © 1998 John Wiley & Sons, Ltd.

KEY WORDS: Navier–Stokes equations; unsteady flow; three-dimensional channel; finite differences; spectral techniques

1. INTRODUCTION

Advances in numerical modelling and computing hardware have provided the possibility of solving complex problems in physics, particularly in fluid mechanics. The system of the non-linear partial differential equations of viscous fluid flow is currently solved by means of complex techniques, in which several different numerical methods are applied in order to develop fast and accurate computational codes. Speed and accuracy are primary objectives to pursue in order to have the possibility of performing numerical simulations at high values of the Reynolds number and, as a consequence, in a framework of fully developed turbulent regime.

The aim of this work is to present a new computational code in which the three-dimensional time-dependent Navier–Stokes equations are solved by means of a mixed spectral–finite difference method. The more general objective of the whole research is to address the problem of turbulence simulation, but this will be a matter for future work: numerical simulation of

* Correspondence to: Dipartimento di Ingegneria Idraulica, Ambientale e del Rilevamento, Politecnico di Milano, Piazza Leonardo da Vinci 32, 20133 Milano, Italy.

CCC 0271–2091/98/110129–14$17.50

Received April 1996
Revised April 1997

turbulence may involve the use of simplified versions of the full Navier–Stokes equations according to the more recent approaches that have been developed on the subject (direct numerical simulation and large eddy simulation [1–3]).

In the following sections, the mathematical formulation and the computational techniques characterizing the code are reported and numerical results are presented at different times and values of the Reynolds number, and compared with results obtained by other authors. The problem considered is the flow of a viscous incompressible fluid in a three-dimensional channel, characterized by two solid walls at $y = \pm 1$ (non-dimensional), (Figure 1). No-slip boundary conditions have been used at the walls, while cyclic conditions have been imposed in the other directions.

The channel flow problem has already been a matter of numerical research for several investigators. Moin and Kim [4] developed a semi-implicit scheme which, with the presence of solid walls, circumvents a numerical difficulty related to the development of a fully explicit pseudospectral method, and presented results at $Re = 100$ (based on centerline velocity and channel half-width). The research work was continued by various authors [5–8] by implementing filtering techniques for the Navier–Stokes equations and perfecting the calculation algorithms. Some of the results reported in this work, are compared with those of Moin and Kim [4].

Direct numerical simulations have been performed by other authors. Orszag and Kells [9] computed plane Poiseuille flows and plane Couette flows at Reynolds numbers up to 5000, by investigating the evolution of finite-amplitude disturbances. Kerr [10] performed a study on the small-scale structures in isotropic turbulence, Spalart [11] simulated the turbulent boundary layer on a flat plate, and Gavrilakis [12] performed calculations of turbulent flow fields in a square duct. More recently, Huser and Biringen [13] also executed a direct numerical simulation of turbulent flow in a square duct at $Re = 600$.

Among the aforementioned works, the results reported by the authors have been produced by computational codes mainly based on finite difference algorithms [6,7,12], codes mainly based on spectral Fourier [10], Fourier–Jacobi [11] or Fourier–Chebyshev formulations [4,8,9], or codes in which mixed spectral–finite difference methods have been employed [13].

Filtering techniques for the Navier–Stokes equations and large eddy simulation approaches have been followed by other researchers. Deardorff [14] performed calculations in the case of the three-dimensional turbulent channel flow, Clark *et al.* [15] performed a study in which subgrid-scale models of different types are compared, and Leslie and Quarini [16] performed an analysis on different approaches for generating subgrid models. Antonopulos-Domis [17] applied the large eddy simulation approach to the problem of mixing a passive scalar in a turbulent flow, Mason and Callen [18] simulated the plane Poiseuille flow problem by using the

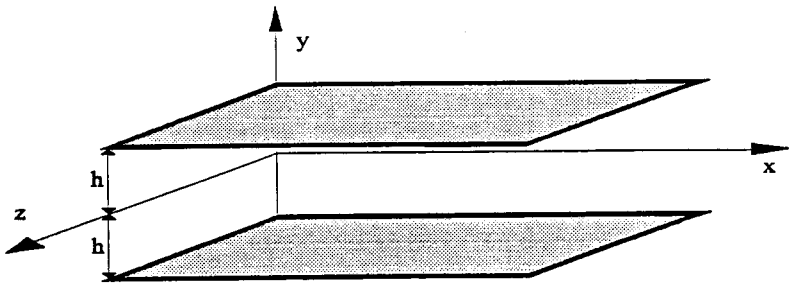

Figure 1. Computational domain.

Smagorinsky model [19] for the subgrid-scale representation. Piomelli *et al.* [20,21] analyzed model consistency and boundary conditions to be applied in large eddy simulations, and later, Piomelli *et al.* [22], Germano *et al.* [23] and Moin *et al.* [24] investigated subgrid-scale models in turbulent compressible and incompressible flow phenomena. Madabhushi and Vanka [25] applied the large eddy simulation technique to the case of the turbulent flow in a square duct and Kaltenbach *et al.* [26], in a recent work (the prosecution of a previous one [27]), used the large eddy simulation approach in a stably stratified shear flow problem. In these works, subgrid-scale models have been applied to the filtered Navier–Stokes equations, in order to explicitly compute the large-scale turbulent flow structures and to model the small-scale ones. The numerical simulations result from computational processes involving Navier–Stokes codes. Finite difference techniques have been mainly used in some of these codes [14,15,17,18], while other codes are built by using mixed spectral–finite difference schemes in their main calculation structure [5,25,26]. Overall, approaches based on mixed techniques still constitute a minority and due to the remarkable versatility characterizing mixed schemes, this approach to the numerical integration of the Navier–Stokes equations is suitable to be followed and further developed.

2. MATHEMATICAL FORMULATION

The system of non-linear partial differential equations in non-dimensional, divergence form and index notation ($i, k = 1, 2, 3$), which governs the flow of a viscous incompressible fluid, is considered

$$\partial_o V_k + \partial_i (V_k V_i) = -\partial_k p + \frac{1}{Re}\partial_i \partial_i V_k, \tag{1a}$$

$$\partial_i V_i = 0, \tag{1b}$$

where the subscript 'o' denotes the partial derivative with respect to time. Below, the co-ordinates x_1, x_2, x_3 and the velocity components V_1, V_2, V_3 will be named x, y, z and u, v, w respectively. Variables and operators have been non-dimensionalized by using the channel half-width (h) as the characteristic length and the steady state centreline velocity ($u_{\max}$) as the characteristic velocity. With reference to Figure 1, the flow fields are admitted to be periodic along the x- and z-directions. Fourier-transforming Equation (1) in those directions gives

$$\frac{\partial \hat{u}}{\partial t} + ik_x \hat{(u^2)} + \frac{\partial (\hat{uv})}{\partial y} + ik_z (\hat{uw}) + ik_x \hat{p} = -\frac{1}{Re} k^2 \hat{u} + \frac{1}{Re}\frac{\partial^2 \hat{u}}{\partial y^2}, \tag{2a}$$

$$\frac{\partial \hat{v}}{\partial t} + ik_x (\hat{vu}) + \frac{\partial \hat{(v^2)}}{\partial y} + ik_z (\hat{vw}) + \frac{\partial \hat{p}}{\partial y} = -\frac{1}{Re} k^2 \hat{v} + \frac{1}{Re}\frac{\partial^2 \hat{v}}{\partial y^2}, \tag{2b}$$

$$\frac{\partial \hat{w}}{\partial t} + ik_x (\hat{wu}) + \frac{\partial (\hat{wv})}{\partial y} + ik_z \hat{(w^2)} + ik_z \hat{p} = -\frac{1}{Re} k^2 \hat{w} + \frac{1}{Re}\frac{\partial^2 \hat{w}}{\partial y^2}, \tag{2c}$$

$$ik_x \hat{u} + \frac{\partial \hat{v}}{\partial y} + ik_z \hat{w} = 0, \tag{2d}$$

where the superscript ' $\wedge$ ' denotes the Fourier transformed variables and $k^2 = k_x^2 + k_z^2$. The non-linear terms in Equation (2a,b,c) must be evaluated by anti-transforming the velocities back to physical space and performing the products. To avoid aliasing errors in the results, the '2/3 rule' has been implemented [28].

To reduce errors of a round-off nature [29], the component u of the physical velocity along x is considered to be the sum of a mean component $\bar{u} = \bar{u}(y, t)$ and a perturbation $u' = u'(x, y, z, t)$. The velocities along y and z do not have mean components because of the mean flow moving with x. The decomposition of u into two parts becomes particularly relevant when values of u^2 with small u' have to be computed. The definition of $\bar{u}$ is selected to obey the following equation and boundary conditions.

$$\frac{\partial \bar{u}}{\partial t} = \frac{1}{Re}\frac{\partial^2 \bar{u}}{\partial y^2} - \left(\overline{\frac{\partial p}{\partial x}}\right), \tag{3}$$

$$\bar{u}(h, t) = 0, \qquad \bar{u}(-h, t) = 0. \tag{4}$$

Equation (2) becomes

$$\frac{\partial \hat{u'}}{\partial t} + ik_x(2\bar{u}\hat{u'} + \hat{u'^2}) + \frac{\partial(\bar{u}\hat{v'} + \hat{u'v'})}{\partial y} + ik_z(\bar{u}\hat{w'} + \hat{u'w'}) + ik_x\hat{p} = -\frac{1}{Re}k^2\hat{u'} + \frac{1}{Re}\frac{\partial^2 \hat{u'}}{\partial y^2}, \tag{5a}$$

$$\frac{\partial \hat{v'}}{\partial t} + ik_x(\bar{u}\hat{v'} + \hat{v'u'}) + \frac{\partial(\hat{v'^2})}{\partial y} + ik_z(\hat{v'w'}) + \frac{\partial \hat{p}}{\partial y} = -\frac{1}{Re}k^2\hat{v'} + \frac{1}{Re}\frac{\partial^2 \hat{v'}}{\partial y^2}, \tag{5b}$$

$$\frac{\partial \hat{w'}}{\partial t} + ik_x(\bar{u}\hat{w'} + \hat{w'u'}) + \frac{\partial(\hat{w'v'})}{\partial y} + ik_z(\hat{w'^2}) + ik_z\hat{p} = -\frac{1}{Re}k^2\hat{w'} + \frac{1}{Re}\frac{\partial^2 \hat{w'}}{\partial y^2},$$

$$ik_x\hat{u'} + \frac{\partial \hat{v'}}{\partial y} + ik_z\hat{w'} = 0. \tag{5d}$$

The convective terms (in x, y and z) and the partial derivatives of the diffusive terms along x and z are then incorporated into the definition of the following expressions [29].

$$C_u(\hat{u'}, \hat{v'}, \hat{w'}, \bar{u}) = ik_x(2\bar{u}\hat{u'} + \hat{u'^2}) + \frac{\partial(\bar{u}\hat{v'} + \hat{u'v'})}{\partial y} + ik_z(\bar{u}\hat{w'} + \hat{u'w'}) + \frac{1}{Re}k^2\hat{u'}, \tag{6a}$$

$$C_v(\hat{u'}, \hat{v'}, \hat{w'}, \bar{u}) = ik_x(\bar{u}\hat{v'} + \hat{v'u'}) + \frac{\partial(\hat{v'^2})}{\partial y} + ik_z(\hat{v'w'}) + \frac{1}{Re}k^2\hat{v'}, \tag{6b}$$

$$C_w(\hat{u'}, \hat{v'}, \hat{w'}, \bar{u}) = ik_x(\bar{u}\hat{w'} + \hat{w'u'}) + \frac{\partial(\hat{w'v'})}{\partial y} + ik_z(\hat{w'^2}) + \frac{1}{Re}k^2\hat{w'}. \tag{6c}$$

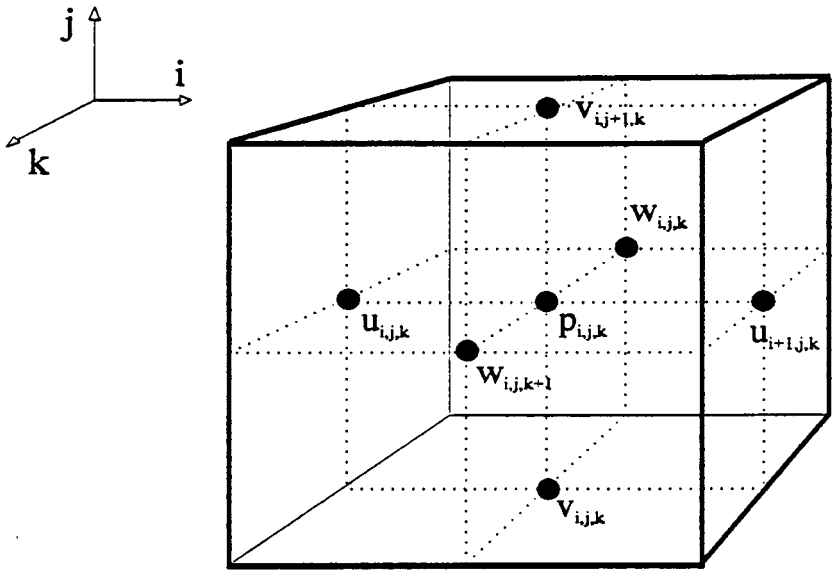

Figure 2. The staggered mesh.

3. COMPUTATIONAL TECHNIQUES

A mixed, semi-implicit technique for the time advancement is devised: a fourth-order Runge–Kutta scheme is used for the terms included in the Equation (6), while second-order centred finite difference implicit schemes of Crank–Nicolson type are implemented on a staggered mesh to handle the partial derivatives of the diffusive terms along y. The staggered mesh allows the pressure to be collocated in the centre of the computational cell, while the three components of the velocity are collocated in the centre of each side of the cell (Figure 2). The following equations hold for each Fourier mode (the partial derivatives with respect to y are still indicated in analytical form)

$$\hat{u}'(t+\Delta t)=\hat{u}'(t)-\frac{1}{6}\Delta t(C_{u_0}+2C_{u_1}+2C_{u_2}+C_{u_3})+\frac{1}{Re}\,\Delta t\,\frac{1}{2}\left(\frac{\partial^2\hat{u}'(t+\Delta t)}{\partial y^2}+\frac{\partial^2\hat{u}'(t)}{\partial y^2}\right)-ik_x\hat{\phi}, \tag{7a}$$

$$\hat{v}'(t+\Delta t)=\hat{v}'(t)-\frac{1}{6}\Delta t(C_{v_0}+2C_{v_1}+2C_{v_2}+C_{v_3})+\frac{1}{Re}\,\Delta t\,\frac{1}{2}\left(\frac{\partial^2\hat{v}'(t+\Delta t)}{\partial y^2}+\frac{\partial^2\hat{v}'(t)}{\partial y^2}\right)-\frac{\partial\hat{\phi}}{\partial y}, \tag{7b}$$

$$\hat{w}'(t+\Delta t)=\hat{w}'(t)-\frac{1}{6}\Delta t(C_{w_0}+2C_{w_1}+2C_{w_2}+C_{w_3})+\frac{1}{Re}\,\Delta t\,\frac{1}{2}\left(\frac{\partial^2\hat{w}'(t+\Delta t)}{\partial y^2}+\frac{\partial^2\hat{w}'(t)}{\partial y^2}\right)-ik_z\hat{\phi}, \tag{7c}$$

$$\bar{u}(t+\Delta t)=\bar{u}(t)+\frac{1}{Re}\,\Delta t\,\frac{1}{2}\left(\frac{\partial^2\bar{u}(t+\Delta t)}{\partial y^2}+\frac{\partial^2\bar{u}(t)}{\partial y^2}\right)-\Delta t\left(\overline{\frac{\partial p}{\partial x}}\right), \tag{7d}$$

where $C_{u_{0,1,2,3}}$, $C_{v_{0,1,2,3}}$, $C_{w_{0,1,2,3}}$ are the forms of C_u, C_v, C_w in the Runge–Kutta procedure, in which the velocities assume intermediate (' $\sim$ ') values ($l = 0, 1, 2, 3$). The following assumptions hold.

$$C_{u_l} = C_u(\tilde{u}_l, \tilde{v}_l, \tilde{w}_l, \bar{u}_l), \qquad C_{v_l} = C_v(\tilde{u}_l, \tilde{v}_l, \tilde{w}_l, \bar{u}_l), \qquad C_{w_l} = C_w(\tilde{u}_l, \tilde{v}_l, \tilde{w}_l, \bar{u}_l) \tag{8}$$

$$u_0 = \bar{u}(t), \qquad \tilde{u}_0 = u'(t), \qquad \tilde{v}_0 = v'(t), \qquad \tilde{w}_0 = w'(t), \tag{9}$$

$$\Delta t_1 = \frac{\Delta t}{2}, \qquad \Delta t_2 = \frac{\Delta t}{2} \qquad \Delta t_3 = \Delta t, \tag{10}$$

and

$$\tilde{u}_l = \hat{u'}(t) - \Delta t_l C_{u_{(l-1)}} + \frac{1}{Re}\,\Delta t_l \frac{1}{2}\left(\frac{\partial^2 \tilde{u}_l}{\partial y^2} + \frac{\partial^2 \hat{u'}(t)}{\partial y^2}\right) - ik_x \hat{\phi}_l, \tag{11a}$$

$$\tilde{v}_l = \hat{v'}(t) - \Delta t_l C_{v_{(l-1)}} + \frac{1}{Re}\,\Delta t_l \frac{1}{2}\left(\frac{\partial^2 \tilde{v}_l}{\partial y^2} + \frac{\partial^2 \hat{v'}(t)}{\partial y^2}\right) - \frac{\partial \hat{\phi}_l}{\partial y}, \tag{11b}$$

$$\tilde{w}_l = \hat{w'}(t) - \Delta t_l C_{w_{(l-1)}} + \frac{1}{Re}\,\Delta t_l \frac{1}{2}\left(\frac{\partial^2 \tilde{w}_l}{\partial y^2} + \frac{\partial^2 \hat{w'}(t)}{\partial y^2}\right) - ik_z \hat{\phi}_l, \tag{11c}$$

$$\bar{u}_l = \bar{u}(t) + \frac{1}{Re}\,\Delta t_l \frac{1}{2}\left(\frac{\partial^2 \bar{u}_l}{\partial y^2} + \frac{\partial^2 \bar{u}(t)}{\partial y^2}\right) - \Delta t_l \left(\overline{\frac{\partial p}{\partial x}}\right), \tag{11d}$$

where $\hat{\phi}_l$ and $\hat{\phi}$ are the Fourier transformed integrals of the pressure over Δt_l and Δt, respectively. Equation (11a,b,c) is manipulated using the procedure of the projection method, as follows. Introducing the additional intermediate variables u_l^*, v_l^*, w_l^* and ψ_l, and imposing mass conservation, gives

$$u_l^* = \hat{u'}(t) - \Delta t_l C_{u_{(l-1)}} + \frac{1}{Re}\,\Delta t_l \frac{1}{2}\left(\frac{\partial^2 u_l^*}{\partial y^2} + \frac{\partial^2 \hat{u'}(t)}{\partial y^2}\right), \tag{12a}$$

$$v_l^* = \hat{v'}(t) - \Delta t_l C_{v_{(l-1)}} + \frac{1}{Re}\,\Delta t_l \frac{1}{2}\left(\frac{\partial^2 v_l^*}{\partial y^2} + \frac{\partial^2 \hat{v'}(t)}{\partial y^2}\right), \tag{12b}$$

$$w_l^* = \hat{w'}(t) - \Delta t_l C_{w_{(l-1)}} + \frac{1}{Re}\,\Delta t_l \frac{1}{2}\left(\frac{\partial^2 w_l^*}{\partial y^2} + \frac{\partial^2 \hat{w'}(t)}{\partial y^2}\right), \tag{12c}$$

at each Runge–Kutta substep; the pressure terms are disconnected from the velocity terms and u_l^*, v_l^*, w_l^* are determined. Then, it is possible to determine ψ_l as a function of the starred velocities, on the basis of the following expression, which is derived from the pressure equation in the form of a Helmholtz equation

$$\frac{\partial^2 \psi_l}{\partial y^2} - k^2 \psi_l = ik_x u_l^* + \frac{\partial v_l^*}{\partial y} + ik_z w_l^*, \tag{13}$$

and the tilded values of the velocity, corrected with the pressure, can be calculated as

$$\tilde{u}_l = u_l^* - ik_x \psi_l, \tag{14a}$$

$$\tilde{v}_l = v_l^* - \frac{\partial \psi_l}{\partial y}, \tag{14b}$$

$$\tilde{w}_l = w_l^* - ik_z\psi_l, \tag{14c}$$

where $\hat{\phi}$ and ψ_l are related by the expression

$$\hat{\phi} = \psi_l - \frac{1}{2}\frac{1}{Re}\,\Delta t_l \frac{\partial^2 \psi_l}{\partial y^2}, \quad l = 3. \tag{15}$$

Equation (15) is obtained by solving any part of Equation (14) in a starred velocity, then substituting the result into the corresponding part of Equation (12) and equating this to the corresponding part of Equation (11a,b,c). Equations (12a,b,c) and (13) are solved numerically using an extensively used algorithm for tridiagonal systems of equations [30].

No-slip boundary conditions at the solid walls and cyclic conditions in the streamwise and spanwise directions have been imposed to the velocity, while boundary conditions of Neumann type have been used for the pressure. In the choice of Δt, we have observed the criterion that the larger value of the CFL number relative to the convective term, is $\leq \sqrt{6}$ [29]. The choices related to both the mathematical formulation of the problem and the numerical techniques are based on the following considerations: (i) the spectral technique has been used in the omogeneous directions (x and z) because of its widely recognized (Reference [31] among others) superiority for the accuracy of the calculations; (ii) a spectral technique could also be used in the direction orthogonal to the solid walls, but in that case it presents disadvantages mainly related to increasing complexity in the resulting algebraic systems and, as a consequence, an increase in the number of operations to be performed [31]; (iii) the use of a finite difference scheme along the y-direction is mainly related to the possibility of locating the collocations points in the more suitable manner (i.e. nearby the walls), according to the spatial resolution that has to be achieved in the numerical simulations (the turbulent scales resolution); (iv) implicit numerical schemes for the time advancement offer the advantage of unconditional stability and the possibility of running the simulations with relatively large time steps; this circumstance is not so relevant in this case, if one considers the fact that the resolution of the fine scales in a turbulent flow also requires a fine resolution in time [3]; for this reason a semi-implicit scheme has been implemented.

4. RELIABILITY OF THE CODE

4.1. Mean velocity $\bar{u} \neq 0$, perturbations = 0

A first series of calculations has been performed under the conditions of absence of perturbation components of the velocity. The algorithms have been advanced in time ($\Delta t = 0.0025$) with the following initial conditions

$$\bar{u} = C(1 - y^8), \tag{16}$$

$$u'(x, y, z) = 0, \qquad v'(x, y, z) = 0, \qquad w'(x, y, z) = 0, \tag{17}$$

where $C = 0.75$ for mass conservation (Equation (16) is first given in Reference [4]). Figures 3 and 4 report the temporal evolution of the mean velocity profile along x at $Re = 100$ and 1000, respectively. The number of grid points is $N_x = 8$, $N_y = 30$ and $N_z = 8$. In both cases the results show a correct process of evolution in time toward the Poiseuille configuration. In Figure 5 the errors $DQ1$ and $DQ2$ in the calculated mass fluxes with an increasing number N_y of

collocation points along y, are reported at $Re = 100$; $DQ1$ is normalized with the mass flux corresponding to the initial velocity profile (16)

$$DQ1 = \frac{\int_{-1}^{+1} \bar{u}(y)\,\mathrm{d}y}{\int_{-1}^{+1} C(1-y^8)\,\mathrm{d}y}. \tag{18a}$$

$DQ2$ is normalized with the theoretical mass flux corresponding to the Poiseuille profile

$$DQ2 = \frac{\int_{-1}^{+1} \bar{u}(y)\,\mathrm{d}y}{\int_{-1}^{+1} C(1-y^2)\,\mathrm{d}y}. \tag{18b}$$

The values of $DQ1$ and $DQ2$ are those corresponding to the steady state condition with that given number of grid points. In both cases, a decrease of the normalized errors in the calculated mass fluxes with the increase of the resolution of the computational grid, is outlined. In particular, the observed trend of the computed variables at different y-resolutions is in good agreement with the results obtained by Le and Moin [7], and reflects the order of the numerical scheme along y.

4.2. Mean velocity $\bar{u} = 0$, perturbations $\neq 0$

A second series of calculations has been performed in the condition of the zero mean velocity component $\bar{u}$. The algorithms have been advanced in time ($\Delta t = 0.0025$) up to $t = 6.25$, with the following initial conditions

$$u'(x, y, z) = \epsilon \frac{L_x}{2} \sin \pi y \cos \frac{4\pi x}{L_x} \sin \frac{2\pi z}{L_z}, \tag{19a}$$

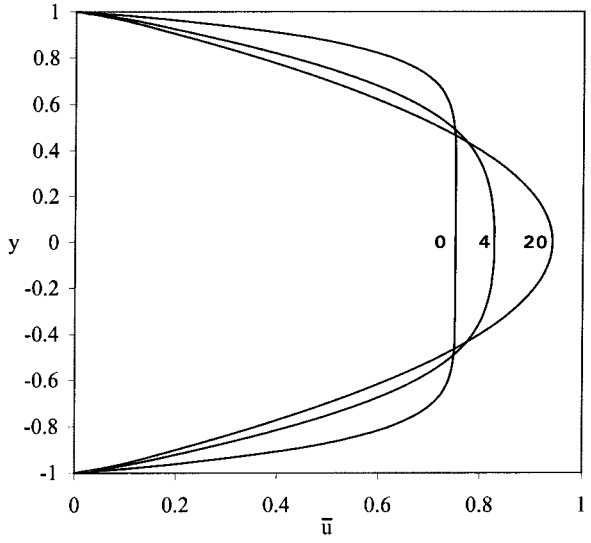

Figure 3. Evolution with time ($t = 0$, 4 and 20) of the mean velocity profile $\bar{u}(y)$ (absence of perturbations, $Re = 100$, $N_x = 8$, $N_y = 30$, $N_z = 8$).

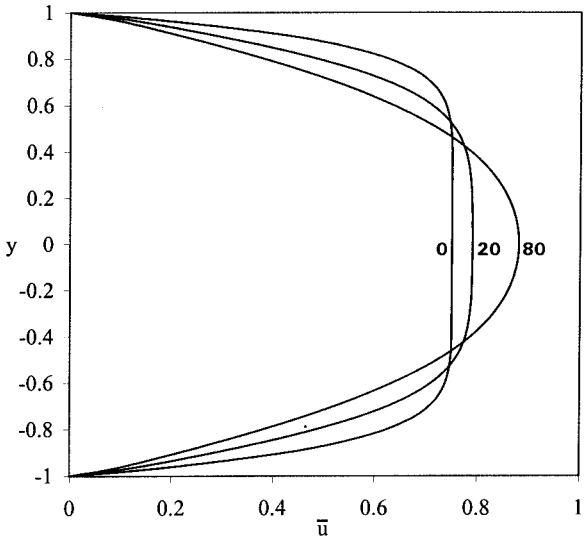

Figure 4. Evolution with time ($t = 0$,20 and 80) of the mean velocity profile $\bar{u}(y)$ (absence of perturbations, Re = 1000, $N_x = 8,\ N_y = 30,\ N_z = 8$).

$$v'(x, y, z) = -\epsilon(1 + \cos \pi y) \sin \frac{4\pi x}{L_x} \sin \frac{2\pi z}{L_z}, \tag{19b}$$

$$w'(x, y, z) = -\epsilon \frac{L_z}{2} \sin \frac{4\pi x}{L_x} \sin \pi y \cos \frac{2\pi z}{L_z}, \tag{19c}$$

where $\epsilon = 0.1$ and $L_x = 2,\ L_z = 2$ represent the linear (dimensionless) dimensions of the computing domain along x and z, respectively. Equation (19) obeys mass conservation and

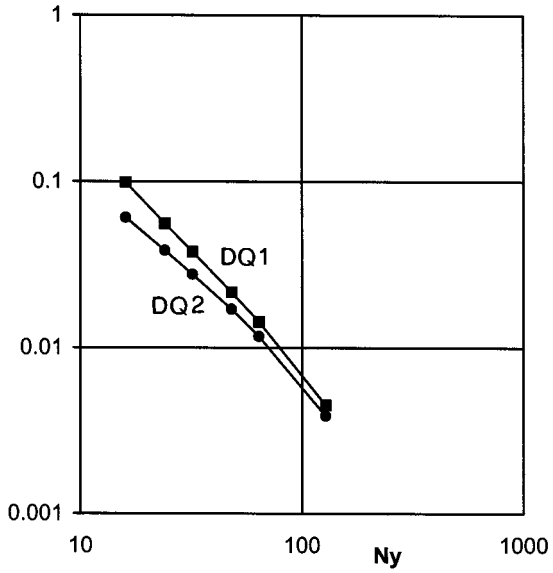

Figure 5. Errors in the calculated mass fluxes $DQ1$ (Equation (18a)) and $DQ2$ (Equation (18b)) with increasing number N_y of collocation points along y (absence of perturbations, $Re = 100$).

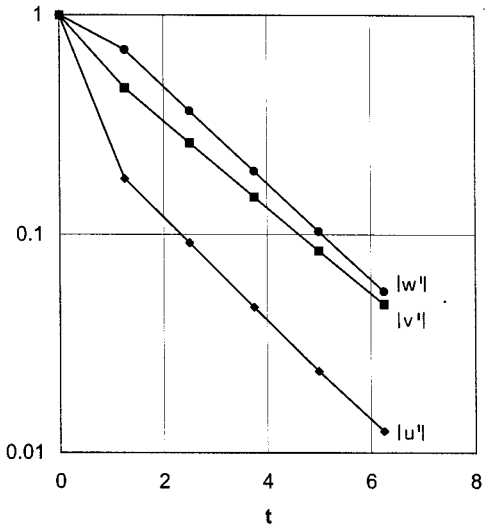

Figure 6. Evolution with time of the perturbation amplitudes $|u'|$, $|v'|$, $|w'|$ at $y = 0$ and $Re = 100$ (absence of mean flow, $N_x = 32$, $N_y = 33$, $N_z = 32$, $\Delta t = 0.0025$).

first appeared in Reference [4]. Figure 6 reports the evolution in time of the maximum amplitude of each of the perturbations (19), normalized with respect to their initial value, at $y = 0$ and $Re = 100$. In Figure 7 the evolution in time of the energy associated with the perturbation components of the velocity (19), is reported

$$E(y, t) = \iint_{L_x L_z} (u'^2 + v'^2 + w'^2)\, \mathrm{d}z\, \mathrm{d}x. \tag{20}$$

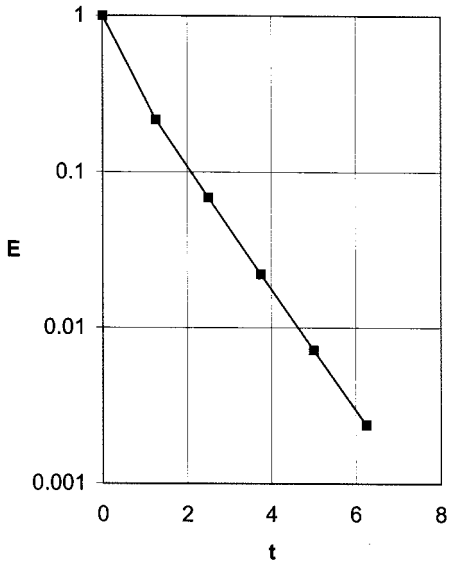

Figure 7. Evolution of the energy $E(y, t)$ (Equation (20)) with time at $y = 0$ and $Re = 100$ (absence of mean flow, $\Delta t = 0.0025$).

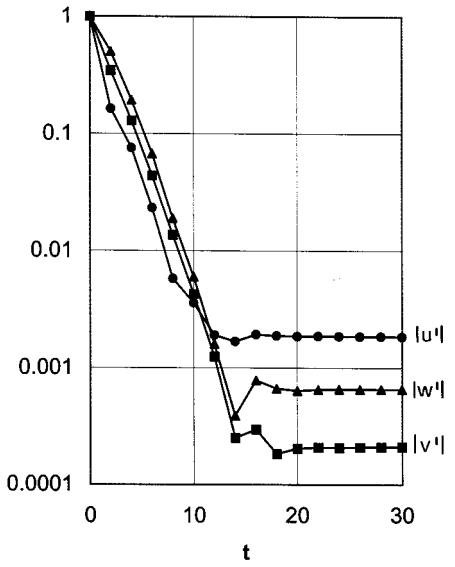

Figure 8. Evolution with time of the perturbation amplitudes $|u'|$, $|v'|$, $|w'|$ at $y = 0$, $Re = 100$ and $N_y = 21$ (presence of mean flow, $N_x = 16$, $N_z = 16$, $\Delta t = 0.0025$).

This is a case (presence of perturbation only) of unforced flow, in which the Reynolds number only has the meaning of a diffusion coefficient. The results reported in Figures 6 and 7 show a correct phenomenon of damping with time of the perturbation amplitudes and of the energy associated with the perturbations, as expected in this type of flow [32].

4.3. Mean velocity $\bar{u} \neq 0$ and perturbations $\neq 0$

A third series of calculations was performed by considering both mean components and perturbation components of the velocity. The algorithms have been advanced in time ($\Delta t = 0.0025$) up to $t = 30$ and the spatial discretization has been tested along y in the process of damping of the perturbation components. In Figure 8 the evolution with time of the maximum value of each of the perturbation amplitudes, normalized with respect to their initial value, is reported at $y = 0$, $Re = 100$ and $N_y = 21$; further calculations at $N_y = 33$ have shown that no remarkable differences between the two tested values of y-discretizations exist. Figure 9 shows the evolution with time of the energy (20) associated with the perturbation components of the velocity at $y = 0$, $Re = 100$ and $N_y = 21$, $N_y = 33$, respectively. Directly after a few non-dimensional times, the values of both perturbation amplitudes and energies drop to negligible entities, for both values of collocation points N_y that have been tested.

This is a case of pressure driven flow in a channel with the presence of three-dimensional disturbances of finite amplitude ($\epsilon = 0.1$); there is not a theory of analytic nature for the non-linear stability of viscous fluid flows. It is also known [33–35] that the existence of disturbances of three-dimensional nature shifts the neutral stability curve toward lower values of the Reynolds number. It is also demonstrated [36] that with Reynolds numbers lower than 1000, any kind of perturbation is damped, as shown in Figures 8 and 9.

In Figure 10, a comparison with the results obtained by Moin and Kim [4] is reported: the temporal evolution of the calculated mean velocity profile shows a satisfactory agreement with their results.

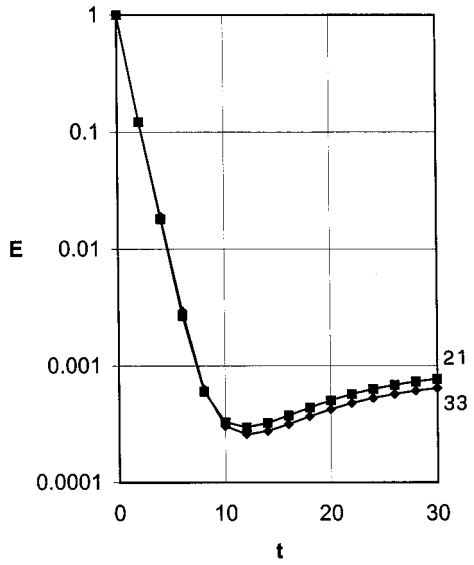

Figure 9. Evolution of the energy $E(y, t)$ (Equation (20)) with time at $y = 0$, $Re = 100$ and $N_y = 21$, $N_y = 33$ (presence of mean flow, $N_x = 16$, $N_z = 16$, $\Delta t = 0.0025$).

5. CONCLUDING REMARKS

A computational code for the numerical integration of the three-dimensional, incompressible Navier–Stokes equations has been developed. The channel flow problem at different values of the Reynolds number has been considered and a mixed spectral–finite difference technique has been implemented, based on Fourier decomposition, second-order Crank–Nicolson algorithms and fourth-order Runge–Kutta schemes. Calculations are performed in the cases of mean flow, perturbation components of the velocity and presence of both mean and perturbation velocities, and they are compared with the results obtained by other authors.

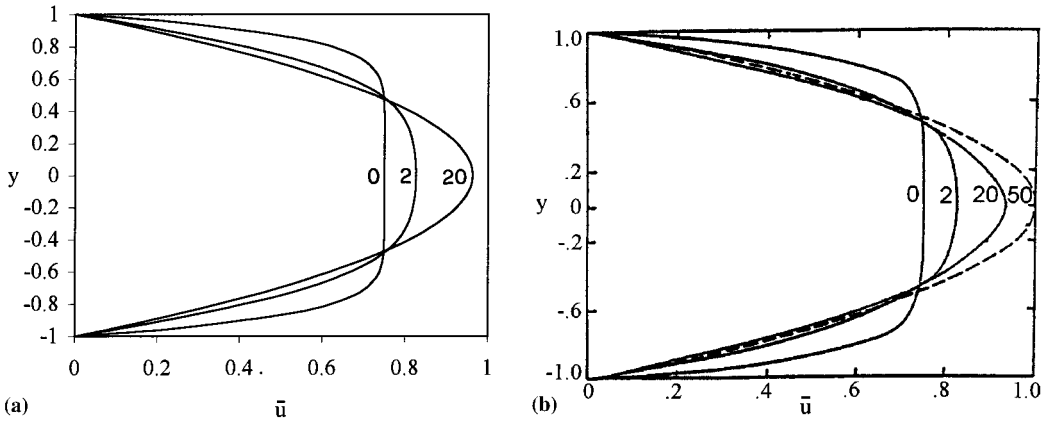

Figure 10. Evolution with time of the mean velocity profile $\bar{u}(y)$. (a) present model ($N_x = 16$, $N_y = 21$, $N_z = 16$, $\Delta t = 0.0025$); (b) results after Moin and Kim [4]. $Re = 100$, based on the channel width.

APPENDIX A. NOMENCLATURE

CFL (number)	Courant–Friedrichs–Lewy (number)
$DQ1$, $DQ2$	normalized errors in the calculated mass flux
E	energy associated to the perturbation components of the velocity
h	channel half-width
k, k_x, k_z	wave numbers
l	index for the Runge–Kutta procedure
L_x, L_y, L_z	length of the computing domain along x, y, z (non-dimensional)
N_x, N_y, N_z	number of grid points along x, y, z
p	fluid pressure (non-dimensional)
Re	Reynolds number
t	time (non-dimensional)
Δt	time step (non-dimensional)
u, v, w	x, y, z components of the velocity (non-dimensional)
u', v',w'	perturbations of u, v, w
$\|u'\|$, $\|v'\|$, $\|w'\|$	maximum amplitudes of u', v', w'
$u_{\max}$	steady state centerline velocity
$\bar{u}$	mean component of u
V	fluid velocity (non-dimensional)
x, y, z	co-ordinates (non-dimensional)

Greek letters

ϵ	multiplicative coefficient in the expressions of u', v' and w'
ϕ, ϕ_l	integral terms for the calculation of the pressure
ψ_l	pressure correction in the projection method

REFERENCES

1. W.C. Reynolds, 'Computation of turbulent flows', *Ann. Rev. Fluid Mech.*, **8**, 183–208 (1976).
2. J.H. Ferziger, 'Large eddy numerical simulations of turbulent flows', *AIAA J.*, **15**, 1261–1267 (1977).
3. R.S. Rogallo and P. Moin, 'Numerical simulation of turbulent flows', *Ann. Rev. Fluid Mech.*, **16**, 99–137 (1984)
4. P. Moin and J. Kim, 'On the numerical solution of time-dependent viscous incompressible fluid flows involving solid boundaries', *J. Comput. Phys.*, **35**, 381–392 (1980).
5. P. Moin and J. Kim, 'Numerical investigation of turbulent channel flow', *J. Fluid Mech.*, **118**, 341–377 (1982).
6. J. Kim and P. Moin, 'Application of a fractional-step method to incompressible Navier–Stokes equations', *J. Comput. Phys.*, **59**, 308–323 (1985).
7. H. Le and P. Moin, 'An improvement of fractional step method for the incompressible Navier–Stokes equations', *J. Comput. Phys.*, **92**, 369–379 (1991).
8. J. Kim, P. Moin and R. Moser, 'Turbulence statistics in fully developed channel flow at low Reynolds number', *J. Fluid Mech.*, **177**, 133–166 (1987).
9. S.A. Orszag and L.C. Kells, 'Transition to turbulence in plane Poiseuille and plane Couette flow', *J. Fluid Mech.*, **96**, 159–205 (1980).
10. R.M. Kerr, 'Higher-order derivative correlations and the alignment of small-scale structures in isotropic numerical turbulence', *J. Fluid Mech.*, **153**, 31–58 (1985).
11. P.R. Spalart, 'Direct simulation of a turbulent boundary layer up to $R_\theta = 1410$', *J. Fluid Mech.*, **187**, 61–98 (1988).
12. S. Gavrilakis, 'Numerical simulation of low-Reynolds-number turbulent flow through a straight square duct', *J. Fluid Mech.*, **244**, 101–129 (1992).

13. A. Huser and S. Biringen, 'Direct numerical simulation of turbulent flow in a square duct', *J. Fluid Mech.*, **257**, 65–95 (1993).
14. J.W. Deardorff, 'A numerical study of three-dimensional turbulent channel flow at large Reynolds numbers', *J. Fluid Mech.*, **41**, 453–480 (1970).
15. R.A. Clark, J.H. Ferziger and W.C. Reynolds, 'Evaluation of subgrid-scale models using an accurately simulated turbulent flow', *J. Fluid Mech.*, **91**, 1–16 (1979).
16. D.C. Leslie and G.L. Quarini, 'The application of turbulence theory to the formulation of subgrid modelling procedures', *J. Fluid Mech.*, **91**, 65–91 (1979).
17. M. Antonopulos-Domis, 'Large-eddy simulation of a passive scalar in isotropic turbulence', *J. Fluid Mech.*, **104**, 55–79 (1981).
18. P.J. Mason and N.S. Callen, 'On the magnitude of the subgrid-scale eddy coefficient in large-eddy simulation of turbulent channel flow', *J. Fluid Mech.*, **162**, 439–462 (1986).
19. J. Smagorinsky, 'General circulation experiments with the primitive equations: 1. The basic experiment', *Monthly Weather Rev.*, **91**, 99–164 (1963).
20. U. Piomelli, P. Moin and J.H. Ferziger, 'Model consistency in large eddy simulation of turbulent channel flow', *Phys. Fluids*, **31**, 1884–1891 (1988).
21. U. Piomelli, J. Ferziger and P. Moin, 'New approximate boundary conditions for large eddy simulations of wall-bounded flows', *Phys. Fluids A*, **1**, 1061–1068 (1989).
22. U. Piomelli, W.H. Cabot, P. Moin and S. Lee, 'Subgrid-scale backscatter in turbulent and transitional flows', *Phys. Fluids A*, **3**, 1766–1771 (1991).
23. M. Germano, U. Piomelli, P. Moin and W.H. Cabot, 'A dynamic subgrid-scale eddy viscosity model', *Phys. Fluids A*, **3**, 1760–1765 (1991).
24. P. Moin, K. Squires, W. Cabot and S. Lee, 'A dynamic subgrid-scale model for compressible turbulence and scalar transport', *Phys. Fluids A*, **3**, 2746–2757 (1991).
25. R.K. Madabhushi and S.P. Vanka, 'Large eddy simulation of turbulence-driven secondary flow in a square duct', *Phys. Fluids A*, **3**, 2734–2745 (1991).
26. H.J. Kaltenbach, T. Gerz and U. Schumann, 'Large-eddy simulation of homogeneous turbulence and diffusion in stably stratified shear flow', *J. Fluid Mech.*, **280**, 1–40 (1994).
27. T. Gerz, U. Schumann and S.E. Elghobashi, 'Direct numerical simulation of stratified homogeneous turbulent shear flows', *J. Fluid Mech.*, **200**, 563–594 (1989).
28. G.S. Patterson and S.A. Orszag, 'Spectral calculations of isotropic turbulence: efficient removal of aliasing interactions', *Phys. Fluids*, **14**, 2538–2541 (1971).
29. A. Wray and M.Y. Hussaini, 'Numerical experiments in boundary-layer stability', *Proc. Roy. Soc. London A*, **392**, 373–389 (1984).
30. W.H. Press, B.P. Flannery, S.A. Teukolsky and W.T. Vetterling, *Numerical Recipes*, Cambridge University Press, Cambridge, 1989.
31. C. Canuto, M.Y. Hussaini, A. Quarteroni and T.A. Zang, *Spectral Methods in Fluid Dynamics*, Springer, Berlin, 1988.
32. H. Tennekes and J.L. Lumley, *A First Course in Turbulence*, MIT Press, Cambridge, 1972.
33. T.W. Kao and C. Park, 'Experimental investigations of the stability of channel flows. Part 1. Flow of a single liquid in a rectangular channel', *J. Fluid Mech.*, **43**, 145–164 (1970).
34. P.S. Klebanoff, K.D. Tidstrom and L.M. Sargent, 'The three-dimensional nature of boundary-layer instability', *J. Fluid Mech.*, **12**, 1–34 (1962).
35. T. Herbert, 'Secondary instability of plane channel flow to subharmonic three-dimensional disturbances', *Phys. Fluids*, **26**, 871–874 (1983).
36. V.C. Patel and M.R. Head, 'Some observations on skin friction and velocity profiles in fully developed pipe and channel flows', *J. Fluid Mech.*, **38**, 181–201 (1969).

